SAND2014-17845PE

Surface plasmon polariton enhanced ultrathin nano-structured CdTe solar cell

Ting S. Luk,[1,2,*] Nche T. Fofang,[1,2] Jose L. Cruz-Campa,[2] Ian Frank,[1,2] and Salvatore Campione[1,2]

[1]*Center for Integrated Nanotechnologies, Sandia National Laboratories, P.O. Box 5800, Albuquerque, NM 87185, USA*

[2]*Sandia National Laboratories, P.O. Box 5800, Albuquerque, NM 87185, USA*

[*] *tsluk@sandia.gov*

Abstract: We demonstrate numerically that two-dimensional arrays of ultrathin CdTe nano-cylinders on Ag can serve as an effective broadband anti-reflection structure for solar cell applications. Such devices exhibit strong absorption properties, mainly in the CdTe semiconductor regions, and can produce short-circuit current densities of 23.4 mA/cm^2, a remarkable number in the context of solar cells given the ultrathin dimensions of our nano-cylinders. The strong absorption is enabled via excitation of surface plasmon polaritons (SPPs) under plane wave incidence. In particular, we identified the key absorption mechanism as enhanced fields of the SPP standing waves residing at the interface of CdTe nano-cylinders and Ag. We compare the performance of Ag, Au, and Al substrates, and observe significant improvement when using Ag, highlighting the importance of using low-loss metals. Although we use CdTe here, the proposed approach is applicable to other solar cell materials with similar absorption properties.

OCIS codes: (310.6628) Subwavelength structures, nanostructures; (240.6680) Surface plasmons; (310.1210) Antireflection coatings.

References and links

1. M. J. de Wild-Scholten, "Energy payback time and carbon footprint of commercial photovoltaic systems," Solar Energy Materials and Solar Cells **119**, 296-305 (2013).
2. J. Britt, and C. Ferekides, "Thin-film CdS/CdTe solar cell with 15.8% efficiency," Applied Physics Letters **62**, 2851-2852 (1993).
3. N. Romeo, A. Bosio, V. Canevari, and A. Podestà, "Recent progress on CdTe/CdS thin film solar cells," Solar Energy **77**, 795-801 (2004).
4. X. Wu, "High-efficiency polycrystalline CdTe thin-film solar cells," Solar Energy **77**, 803-814 (2004).
5. S. Mokkapati, F. J. Beck, A. Polman, and K. R. Catchpole, "Designing periodic arrays of metal nanoparticles for light-trapping applications in solar cells," Applied Physics Letters **95**, - (2009).
6. S. Pillai, K. R. Catchpole, T. Trupke, and M. A. Green, "Surface plasmon enhanced silicon solar cells," Journal of Applied Physics **101**, - (2007).
7. H. A. Atwater, and A. Polman, "Plasmonics for improved photovoltaic devices," Nat Mater **9**, 205-213 (2010).
8. S. Pillai, F. J. Beck, K. R. Catchpole, Z. Ouyang, and M. A. Green, "The effect of dielectric spacer thickness on surface plasmon enhanced solar cells for front and rear side depositions," Journal of Applied Physics **109**, - (2011).
9. K. R. Catchpole, and A. Polman, "Plasmonic solar cells," Opt. Express **16**, 21793-21800 (2008).
10. V. E. Ferry, M. A. Verschuuren, H. B. T. Li, R. E. I. Schropp, H. A. Atwater, and A. Polman, "Improved red-response in thin film a-Si:H solar cells with soft-imprinted plasmonic back reflectors," Applied Physics Letters **95**, - (2009).
11. N. T. Fofang, T. S. Luk, M. Okandan, G. N. Nielson, and I. Brener, "Substrate-modified scattering properties of silicon nanostructures for solar energy applications," Opt. Express **21**, 4774-4782 (2013).
12. P. Spinelli, M. A. Verschuuren, and A. Polman, "Broadband omnidirectional antireflection coating based on subwavelength surface Mie resonators," Nat Commun **3**, 692 (2012).

13. S. Jeong, E. C. Garnett, S. Wang, Z. Yu, S. Fan, M. L. Brongersma, M. D. McGehee, and Y. Cui, "Hybrid Silicon Nanocone–Polymer Solar Cells," Nano Letters **12**, 2971-2976 (2012).
14. K. X. Wang, Z. Yu, V. Liu, Y. Cui, and S. Fan, "Absorption Enhancement in Ultrathin Crystalline Silicon Solar Cells with Antireflection and Light-Trapping Nanocone Gratings," Nano Letters **12**, 1616-1619 (2012).
15. J. Zhu, C.-M. Hsu, Z. Yu, S. Fan, and Y. Cui, "Nanodome Solar Cells with Efficient Light Management and Self-Cleaning," Nano Letters **10**, 1979-1984 (2009).
16. J. Zhu, Z. Yu, G. F. Burkhard, C.-M. Hsu, S. T. Connor, Y. Xu, Q. Wang, M. McGehee, S. Fan, and Y. Cui, "Optical Absorption Enhancement in Amorphous Silicon Nanowire and Nanocone Arrays," Nano Letters **9**, 279-282 (2008).
17. J. K. Day, O. Neumann, N. K. Grady, and N. J. Halas, "Nanostructure-Mediated Launching and Detection of 2D Surface Plasmons," ACS Nano **4**, 7566-7572 (2010).
18. H. Ditlbacher, J. R. Krenn, A. Hohenau, A. Leitner, and F. R. Aussenegg, "Efficiency of local light-plasmon coupling," Applied Physics Letters **83**, 3665-3667 (2003).
19. L. Xin, H. Dezhuan, W. Fengqin, X. Chun, L. Xiaohan, and Z. Jian, "Flat metallic surfaces coated with a dielectric grating: excitations of surface plasmon–polaritons and guided modes," Journal of Physics: Condensed Matter **20**, 485001 (2008).
20. I. P. Radko, S. I. Bozhevolnyi, G. Brucoli, L. Martín-Moreno, F. J. García-Vidal, and A. Boltasseva, "Efficiency of local surface plasmon polariton excitation on ridges," Physical Review B **78**, 115115 (2008).
21. I. P. Radko, S. I. Bozhevolnyi, G. Brucoli, L. Martin-Moreno, F. J. Garcia-Vidal, and A. Boltasseva, "Efficient unidirectional ridge excitationof surface plasmons," Opt. Express **17**, 7228-7232 (2009).
22. S. Randhawa, M. U. González, J. Renger, S. Enoch, and R. Quidant, "Design and properties of dielectric surface plasmon Bragg mirrors," Opt. Express **18**, 14496-14510 (2010).
23. J. Yoon, G. Lee, S. H. Song, C.-H. Oh, and P.-S. Kim, "Surface-plasmon photonic band gaps in dielectric gratings on a flat metal surface," Journal of Applied Physics **94**, 123-129 (2003).
24. N. I. Landy, S. Sajuyigbe, J. J. Mock, D. R. Smith, and W. J. Padilla, "Perfect Metamaterial Absorber," Physical Review Letters **100**, 207402 (2008).
25. M. Pu, Q. Feng, C. Hu, and X. Luo, "Perfect Absorption of Light by Coherently Induced Plasmon Hybridization in Ultrathin Metamaterial Film," Plasmonics **7**, 733-738 (2012).
26. I. Staude, A. E. Miroshnichenko, M. Decker, N. T. Fofang, S. Liu, E. Gonzales, J. Dominguez, T. S. Luk, D. N. Neshev, I. Brener, and Y. Kivshar, "Tailoring Directional Scattering through Magnetic and Electric Resonances in Subwavelength Silicon Nanodisks," ACS Nano **7**, 7824-7832 (2013).
27. K. R. Catchpole, and M. A. Green, "A conceptual model of light coupling by pillar diffraction gratings," Journal of Applied Physics **101**, - (2007).
28. K. R. Catchpole, and A. Polman, "Design principles for particle plasmon enhanced solar cells," Applied Physics Letters **93**, - (2008).
29. V. E. Ferry, M. A. Verschuuren, H. B. T. Li, E. Verhagen, R. J. Walters, R. E. I. Schropp, H. A. Atwater, and A. Polman, "Light trapping in ultrathin plasmonic solar cells," Opt. Express **18**, A237-A245 (2010).
30. W. Liu, A. E. Miroshnichenko, D. N. Neshev, and Y. S. Kivshar, "Broadband Unidirectional Scattering by Magneto-Electric Core–Shell Nanoparticles," ACS Nano **6**, 5489-5497 (2012).
31. N. A. Mirin, and N. J. Halas, "Light-Bending Nanoparticles," Nano Letters **9**, 1255-1259 (2009).
32. S. J. Oldenburg, G. D. Hale, J. B. Jackson, and N. J. Halas, "Light scattering from dipole and quadrupole nanoshell antennas," Applied Physics Letters **75**, 1063-1065 (1999).
33. G. Pellegrini, P. Mazzoldi, and G. Mattei, "Asymmetric Plasmonic Nanoshells as Subwavelength Directional Nanoantennas and Color Nanorouters: A Multipole Interference Approach," The Journal of Physical Chemistry C **116**, 21536-21546 (2012).
34. E. Xifré-Pérez, L. Shi, U. Tuzer, R. Fenollosa, F. Ramiro-Manzano, R. Quidant, and F. Meseguer, "Mirror-Image-Induced Magnetic Modes," ACS Nano **7**, 664-668 (2012).
35. B. Aguirre, D. Zubia, R. Ordonez, F. Anwar, H. Prieto, C. Sanchez, M. Salazar, A. A. Pimentel, J. Michael, X. Zhou, J. McClure, G. Nielson, and J. Cruz-Campa, "Selective Growth of CdTe on Nano-patterned CdS via Close-Space Sublimation," Journal of Elec Materi **43**, 2651-2657 (2014).
36. I. B. Bhat, S. R. Rao, S. Shintri, and R. N. Jacobs, "Blanket and patterned growth of CdTe on (211)Si substrates by metal-organic vapor phase epitaxy," physica status solidi (c) **9**, 1712-1715 (2012).
37. S. Shintri, S. Rao, C. Schaper, W. Palosz, S. Trivedi, F. Semendy, P. Wijewarnasuriya, and I. Bhat, "Metalorganic vapor phase epitaxial growth of (211)B CdTe on nanopatterned (211)Si," physica status solidi (c) **9**, 1716-1719 (2012).
38. J. J. Chavez, D. K. Ward, B. M. Wong, F. P. Doty, J. L. Cruz-Campa, G. N. Nielson, V. P. Gupta, D. Zubia, J. McClure, and X. W. Zhou, "Defect formation dynamics during CdTe overlayer growth," Physical Review B **85**, 245316 (2012).
39. E. D. Palik, *Handbook of Optical Constants of Solids* (Academic Press, 1991).
40. P. Wurfel, *Physics of Solar Cells* (Wiley-VCH Verlag, 2009).
41. J. L. Cruz-Campa, G. N. Nielson, P. J. Resnick, M. Okandan, R. Young, D. Zubia, and V. Gupta, "Ultrathin and micro-sized solar cell performance optimization via simulations," Progress in photovoltaics: research and applications **21**, 1114-1126 (2013).

42. J. L. Cruz-Campa, M. Okandan, P. J. Resnick, P. Clews, T. Pluym, R. K. Grubbs, V. P. Gupta, D. Zubia, and G. N. Nielson, "Microsystems enabled photovoltaics: 14.9% efficient 14 mu m thick crystalline silicon solar cell," Sol. Energy Mater. Sol. Cells **95**, 551-558 (2011).

1. Introduction

Cadmium telluride (CdTe) based solar cells have the lowest carbon footprint, production cost, shortest cost recovery, and competitive performance when compared against their Si counterpart [1]. CdTe is a direct band gap semiconductor material with the band gap energy of 1.44 eV, similar to GaAs. While the required absorption thickness for direct band gap materials is of the order of 1-10 micrometers, it is still advantageous to reduce the thickness further to minimize cadmium content and tellurium usage per panel and improve carrier extraction. In addition, absorption can be improved if the Fresnel reflection is reduced. However, standard single layer anti-reflection coatings are ineffective for broadband reflection reduction [2-4]. For this reason, light scattering of nano-patterned plasmonic structures that enhance light trapping and hence absorption has been previously proposed to improve solar cells performance [5-10]. However, most of the reported structures used nano-patterned metal structures or plasmonic nanoparticles as scatterers [7, 11-23] to trap light in the material where electron-hole pairs are generated.

In contrast the structure studied in this paper uses nano-patterned semiconductors as scatterers on a continuous metal surface to enable surface plasmon polariton (SPP) excitations which facilitate enhanced absorption and serve as an anti-reflection coating [11, 12]. In particular, we aim to design ultrathin structured surfaces of CdTe nano-particles exhibiting simultaneously broadband anti-reflection and strong absorption properties through surface impedance matching to free space [5, 6, 11, 24-26]. We adopt a nano-patterned surface made of CdTe nano-cylinders on Ag as shown in Fig. 1(a). Light reflection properties created by this surface are controlled by the scattering properties of the nano-cylinders through size and shape control. The scattered field of the nano-particles produces enhanced coupling to optical modes in the structure and hence absorption enhancement [5, 7, 8, 11, 27-34]. Another advantage of using nano-patterned [35] solar cells is to reduce defect concentration during deposition or crystal growth [36, 37]. Defect creation induced by strain and lattice mismatch is less likely when the area and growth thickness is reduced [38].

The paper is organized as follows. We introduce the proposed nano-patterned structure in Sec. 2, where we show that the key absorption mechanism owes its origin to the SPP standing waves residing at the interface of CdTe nano-cylinders and Ag. We then show in Sec. 3 that most of the absorbed energy resides in the semiconductor regions, making the proposed device appealing for solar cell applications. We eventually complete the photovoltaic circuit by adding a second conducting electrode. Finally, we draw conclusions in Sec. 4.

2. Arrays of CdTe nano-cylinders as scatterers for SPP excitation and enhanced absorption

The structure analyzed here is shown in Fig. 1(a) where an ultrathin (110 nm) CdTe film placed on an optically thick continuous Ag film is patterned into a nano-cylinder array. We found that this thickness is necessary to provide optimum scattering strength to couple the external plane wave efficiently to the SPP. The nano-cylinders, with diameters of 340 nm, are arranged in a square lattice with a period of 440 nm. Under normal incidence of *x*-polarized light from air to the structure [see Fig. 1(a)], the reflectivity *R*, reported as a blue curve in Fig. 1(b), shows near zero values (about 7% on average) from ~0.85 μm (the onset of the band edge) to ~0.45 μm. Therefore, the absorption – obtained by calculating 1-*R* – is very close to 1 in a wide frequency band in the solar spectrum. In contrast, the reflectivity of an unpatterned film in the same spectral region is much higher, as shown by the red curve in Fig

1(b). This corresponds to a much lower absorption in the same spectral band. The electric field intensity pattern at the wavelength of 0.8 μm obtained from full-wave finite-difference time-domain simulations (FDTD Solutions by Lumerical Solutions Inc.) is shown in Fig. 1(c). The CdTe dielectric constant used in simulation is obtained from the database of a J.A. Woollam ellipsometer, whereas the Ag permittivity values are from Palik [39]. The enhanced field patterns at the surface of the Ag/CdTe interface and at the air gap between nano-cylinders suggest excitation of SPP induced by scattering of the CdTe nano-cylinder array.

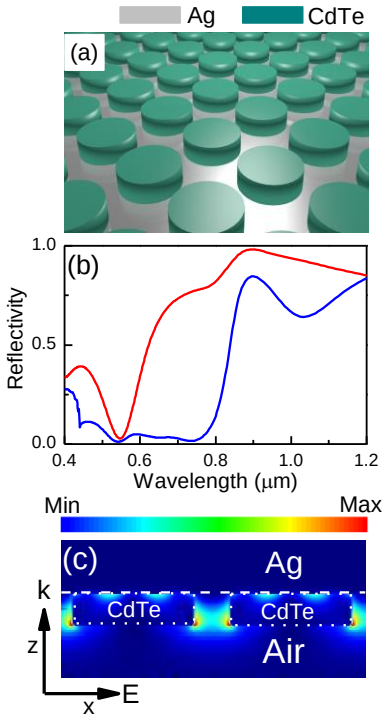

Fig. 1. (a) 3D schematic of an array of CdTe nano-cylinders on Ag substrate. The CdTe nano-cylinders have a diameter of 340 nm and a height of 110 nm. The periodicity is 440 nm. (b) Reflectivity spectrum of the nano-patterned structure of CdTe nano-cylinders on Ag substrate (blue curve) and unpatterned CdTe thin film with the nano-cylinders' thickness (red curve) from normal incidence plane waves. (c) Electric field intensity plots at the wavelength of 0.8 μm. The plot shows intense fields between CdTe nano-cylinders (dotted rectangles) and also at the interface between the CdTe nano-cylinders and Ag (white dash line). The intense fields at the interface of CdTe and Ag pertain to SPPs.

In order to verify whether these modes on the CdTe/Ag interface are indeed SPP modes, we compare the dispersion curves of these modes in two different situations, both shown in Fig. 2(a): (1) CdTe nano-cylinders and (2) an unpatterned CdTe film, both on top of an Ag substrate. First, each point on the dispersion curve for case (1) is obtained by determining the in-plane wavenumber ($k_{//}$) of the SPP mode from the spatial separation of the field maxima pertaining to a given excitation frequency. Field patterns of several excitation wavelengths are shown in Figs. 2(b)-2(d). The dispersion curve is obtained by repeating this analysis for different incident wavelengths and is shown by red dots in Fig. 2(a). Second, the dispersion curve of the SPP for case (2) is instead obtained by using photonic bandstructure simulations; the result is shown as blue diamonds in Fig. 2(a). The two dispersion curves are similar and thus confirm that the field patterns on the CdTe/Ag interface are due to SPP excitations in

both cases. Hence, this shows the broadband coupling to SPP is provided by the scattering of the CdTe nano-cylinder array.

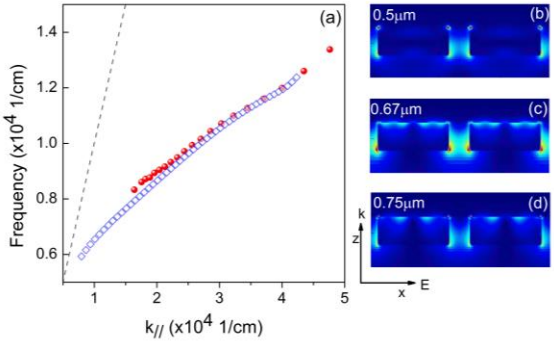

Fig. 2. (a) SPP dispersion obtained from FDTD simulations of an array of CdTe nano-cylinders on Ag substrate (red dots) and unpatterned CdTe thin film on Ag substrate (blue diamonds). The red dots are obtained by extracting SPP wavelengths from electric field intensity plots such as shown in (b-d). The dash gray line represents the light line in air. (b)-(d) Electric field intensity plots at wavelengths: 0.5 μm, 0.67 μm and 0.75 μm. Color map of the field is as in Fig. 1(c).

3. Absorption spatial distribution: most energy resides in the CdTe semiconductor regions

Next, we determine where the energy is being absorbed in the case of an array of CdTe nano-cylinders on a metallic substrate. Again, using FDTD simulations, we place absorption monitors in separate spatial regions: (1) the metal region, and (2) the CdTe region. The local absorbed power density P_{abs} is computed from the field using $P_{abs}(x,y,z)=0.5\omega\varepsilon''|\mathbf{E}(x,y,z)|^2$, where ε'' is the imaginary part of the absolute dielectric constant of the material, ω and **E** are the angular frequency and electric field respectively. For this simulation, we consider Ag, Au, and Al substrates in order to show the importance of low-loss plasmonic materials, and the results are shown in Figs. 3(a), 3(b), and 3(c), respectively. When considering the Ag substrate, about 90% of the total absorption occurs in the CdTe region in the band ~0.40-0.861 μm as shown in Fig 3(a) (blue trace), whereas the Ag contribution accounts for only about 10% of the total absorption, as represented by the green trace. The sum of these absorptions [Fig. 3(a), red trace] is in good agreement with the total absorption obtained from reflectivity calculations [Fig. 3(a), black trace] computed as 1-*R*. Replacing Ag with Au [Fig. 3(b)] or Al [Fig. 3(c)] reduces the absorption in CdTe considerably. Au and Ag have similar plasma frequencies and hence the overall reflectivity responses of the two structures are similar. However, since Au has larger losses than Ag as indicated by a larger ε'', more energy is absorbed in Au. Regarding Al, which has a different plasma frequency and a strong absorption feature around 0.8 μm, the reflectivity response and the ratio of the absorbed energy in CdTe and metal are very different from the case of Ag. Therefore, low-loss metals enable stronger field enhancements in CdTe and hence stronger absorption and simultaneously smaller loss in the metal. Based on these CdTe absorption spectra, we computed the short-circuit current densities [40] using the AM1.5 solar spectrum in the wavelength range from 0.4 μm to 0.861 μm for Ag, Au and Al as plasmonic material and obtained 23.2, 20.6 and 18.8 mA/cm^2 respectively. This is a significant increase from the short-circuit current density of 15 mA/cm^2 from an unpatterned CdTe film on Ag and is comparable to the theoretical maximum of 29.5 mA/cm^2 [4]. Moreover, we stress again that in our structure we obtain these current density values with ultrathin nano-cylinders.

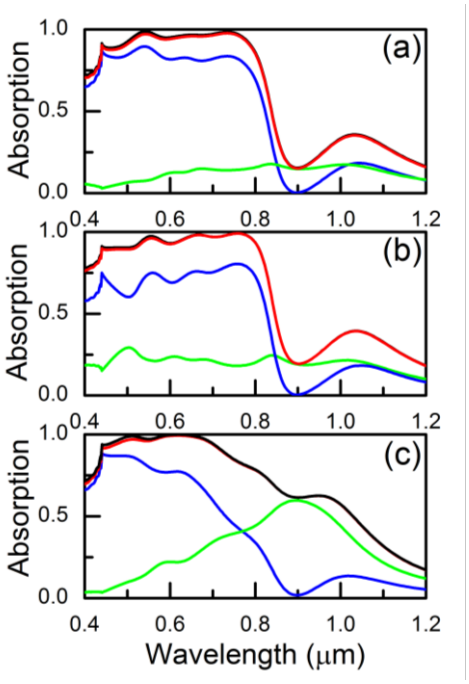

Fig. 3. Absorption spectra of arrays of CdTe nano-cylinders on (a) Ag, (b) Au, and (c) Al substrates. The contribution from CdTe (blue), metal (green), and total absorption (red) are separately shown. As expected, the total absorption in red is identical to that obtained from 1-*R* (black).

We then show the spectral and spatial distribution of the absorption in the CdTe material. As mentioned before, the field energy is concentrated near the CdTe/Ag interface and hence strong absorption takes place near the Ag surface. The location of field maxima in the CdTe changes with incident excitation wavelength. Figure 4(a) helps to visualize this concept; we assemble a series of field intensity profiles at different wavelengths spanning the *x*-coordinate in a unit cell, at a distance of 10 nm from the CdTe/Ag interface cutting through the nano-cylinder. We can clearly see from Figs. 2(b)-2(d) that a standing SPP wave pattern is created inside the CdTe nano-cylinder. As the wavelength is decreased, we see in Fig. 4(a) that higher order modes supporting 4 antinodes start to emerge. The SPP mode disappears at wavelengths shorter than 600 nm. This is due to strong damping of the SPP as its frequency approaches $\omega_p/\sqrt{(\varepsilon_\infty+\varepsilon_{CdTe})}$, ε_∞ and ω_p are the DC dielectric constant and angular plasma frequency of Ag respectively, and ε_{CdTe} is the dielectric constant of CdTe. In such cases, the SPP wave is localized and strongly damped at the edge of the nano-cylinder and is unable to establish standing wave inside the nano-cylinder. This suggests standing wave patterns play a key role in the enhanced absorption mechanism. The local energy map can be created by evaluating the P_{abs} expression described earlier and is shown in Fig. 4(b). As mentioned, the low-wavelength cut-off is due to strong damping resulting in weak field enhancement. Here, we also see the high-wavelength cut-off is due to the band gap of the CdTe material where ε'' is small.

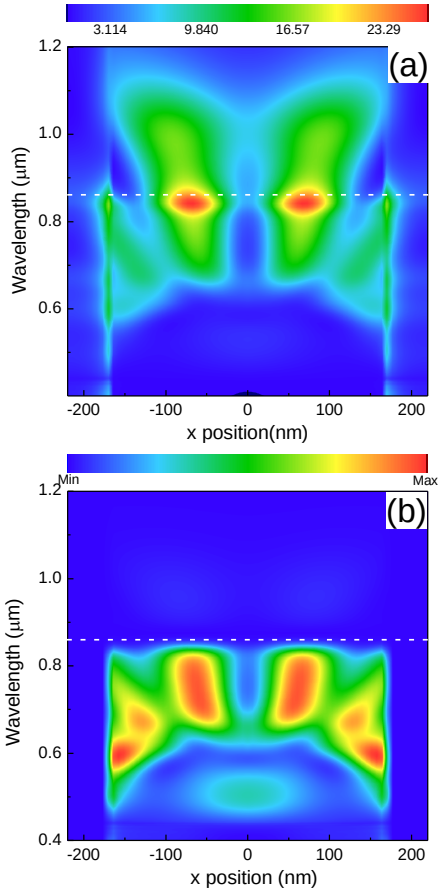

Fig. 4. (a) Field intensity enhancement versus wavelength and *x*-coordinate in a unit cell at a distance of 10 nm from the CdTe/Ag interface cutting through the nano-cylinder. The *x*-axis spans one period (440 nm) of the structure. (b) Similar to (a), showing the spatial absorption contour. It is evident that most of the absorption resides within the CdTe nano-cylinders. The white dash line shows the location of the CdTe band edge.

Finally, to complete the photovoltaic circuit, a second conducting electrode is implemented by a planar layer of a conductive oxide [e.g. indium tin oxide (ITO)] and insulating oxide (e.g. SiO_2) films between the nano-cylinders on top of the Ag substrate with a total thickness of 20 nm as shown in the inset of Fig. 5. The inset in Fig. 5 is a simplified version of the structure and is not intended to depict an actual electronic device. If a device were to be built, an n-doped material such as CdS should be introduced between CdTe and ITO. This configuration provides electrical contact only on the curved lateral surface of the CdTe nano-cylinders. For the sake of computing the short-circuit current density accurately, the conductive and insulating oxides are considered as lossless dielectrics with indices of refraction of 1.6 and 1.4, respectively. These additional films modified the optimal nano-cylinder design, which now requires a diameter of 360 nm and a height of 170 nm, producing a short-circuit current density of 23.4 mA/cm^2, comparable to the value relative to the design in Fig. 3(a) because of the larger CdTe absorption at larger wavelengths in Fig. 5, and still significantly larger than what can be achieved using an unpatterned CdTe film on Ag.

Similar to what was done in Fig. 3, we plot in Fig. 5 the absorption spectra in the CdTe and Ag regions of this structure. Because the conductive film is very thin, the resistivity of this material is higher than the value needed for efficient conduction, which is typically 10^{-4}

Ωcm. However, it may be possible to trade optical transmission for lower resistivity with higher tin concentration in the ITO since this material is not directly in the light path. In addition, while photocurrent is the main target of this research, the photovoltage of a cell is also an important parameter. The loss of voltage encountered in small and thin solar cells has been mainly attributed to edge effects, increased dark currents, and surface recombination [41]. Nonetheless, it has been shown that careful engineering of the passivation in thin films can lead to comparable levels of voltage as their thicker counterparts [42].

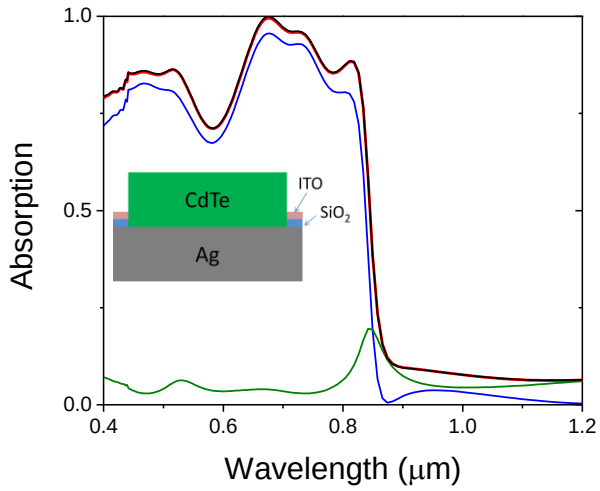

Fig. 5. Absorption spectra as in Fig. 3(a) for a complete photovoltaic circuit obtained including a second conducting electrode implemented with insulating SiO_2 and conductive ITO as shown in the inset. Here, ITO and SiO_2 are treated as lossless dielectrics.

4. Conclusion

In summary, we have shown that nano-patterned CdTe nano-cylinders on metallic substrates can lead to broadband, strong absorption throughout the solar spectrum. Low-loss metals like Ag lead to better absorption performance. We further identified the key absorption mechanism through the coupling to the standing SPP mode inside the CdTe nano-cylinders. Most of the energy is absorbed within the CdTe regions, leading to larger short-circuit current densities than what is achievable in an unpatterned structure on Ag. These results provide guidance to enhance solar cell performance of CdTe or other materials with similar properties.

Acknowledgments

The authors acknowledge fruitful discussion with Dr. Igal Brener. This work was supported by Sandia National Laboratory Directed Research Development and, in part, by the Center for Integrated Nanotechnologies, a U.S. Department of Energy, Office of Basic Energy Sciences user facility. Sandia National Laboratories is a multi-program laboratory managed and operated by Sandia Corporation, a wholly owned subsidiary of Lockheed Martin Corporation, for the U.S. Department of Energy's National Nuclear Security Administration under contract DE-AC04-94AL85000.